Carrier-mediated ferromagnetism in p-Si(100) by sequential ion-implantation of B and Mn

2008 J. Phys.: Condens. Matter 20 095004

(http://iopscience.iop.org/0953-8984/20/9/095004)

J. Phys.: Condens. Matter **20** (2008) 095004 (6pp) doi:10.1088/0953-8984/20/9/095004

Carrier-mediated ferromagnetism in p-Si(100) by sequential ion-implantation of B and Mn

Hung-Ta Lin[1], **Wei-Ji Huang**[1], **Shuo-Hong Wang**[1], **Hsiu-Hau Lin**[2] **and Tsung-Shune Chin**[1,3,4]

[1] Department of Materials Science and Engineering, National Tsing Hua University, 101, Section 2, Kuang-Fu Road, Hsinchu 30013, Taiwan
[2] Department of Physics, National Tsing Hua University, Hsinchu 30013, Taiwan
[3] Department of Materials Science and Engineering, Feng Chia University, 100, Wenhwa Road, Seatwen District, Taichung 40724, Taiwan

E-mail: tschin@mx.nthu.edu.tw

Received 23 August 2007, in final form 19 December 2007
Published 8 February 2008
Online at stacks.iop.org/JPhysCM/20/095004

Abstract

Ferromagnetic $Si_{1-x}Mn_x$ was prepared by implanting B^+ and Mn^+ ions in sequence into p-type Si(100) at room temperature and post-annealing at 700–900 °C. Superparamagnetic nano-sized silicide precipitates, 10–27 at.% Mn, were found near the surface of all $Si_{1-x}Mn_x$ samples. Annealing at 800 °C or below leads to the formation of a thin Si(Mn) layer, with 1.1 at.% Mn, ∼180 nm beneath the surface, giving rise to ferromagnetism with a Curie temperature above 250 K. The high-temperature ferromagnetism is attributed to the indirect exchange mediated by localized carriers in the impurity states. The Mn content of 1–1.5 at.%, having been separately reported to show room-temperature ferromagnetism several times by different groups, seems meaningful for Si-based diluted magnetic semiconductors (DMS). Possible extensions of our work presented here are elucidated.

(Some figures in this article are in colour only in the electronic version)

1. Introduction

Spintronics [1, 2], which is an interdisciplinary field including semiconductors, magnetism, optics and related studies, provides great potential for next-generation devices with characteristics of high-speed information manipulation and low operating power. In particular, one of the exciting developments in recent years is the successful fabrication of diluted magnetic semiconductors (DMS) by doping transition metals such as Mn, Co, and Ni into nonmagnetic semiconductors [3, 4]. Combining together semiconductor and magnetic properties, these novel materials open up the possibility of replacing ferromagnetic metals overcoming the notorious interfacial problem in polarized spin injection [5, 6]. For instance, the widely studied III–V DMS $Ga_{1-x}Mn_xAs$ [7] and the II–VI $Zn_{1-x}Co_xO$ [8–10] have successfully been made into model devices for spin-current injection [11] and spin field-effect transistors [12], which operate rather well at low temperatures.

To be compatible with the existing semiconductor industry, there is also strong interest in DMS based on group IV host semiconductors like $Ge_{1-x}Mn_x$ [13–18] and $Si_{1-x}Mn_x$ [19–29]. Recent reports on $Si_{1-x}Mn_x$, fabricated by means of ion implantation, showed ferromagnetic characteristics with a Curie temperature (T_C) ranging from 70 to 400 K [19–25]. Of particular interest is the effectiveness of ion implantation at low temperature [24], as well as Si nanowires [25]. $Si_{1-x}Mn_x$ films prepared by molecular beam epitaxy or magnetron sputtering have been claimed to exhibit a T_C around room temperature [26, 28, 29]. Although there have been promising reports on room-temperature ferromagnetism of Mn-doped Si, we believe that the experimental outcomes are in fact rather scattered and seem to depend on the detailed growth method and conditions, at least at the point of writing, counting the vast number of unpublished papers with low Curie temperatures. Inspired by the potential

[4] Author to whom any correspondence should be addressed.

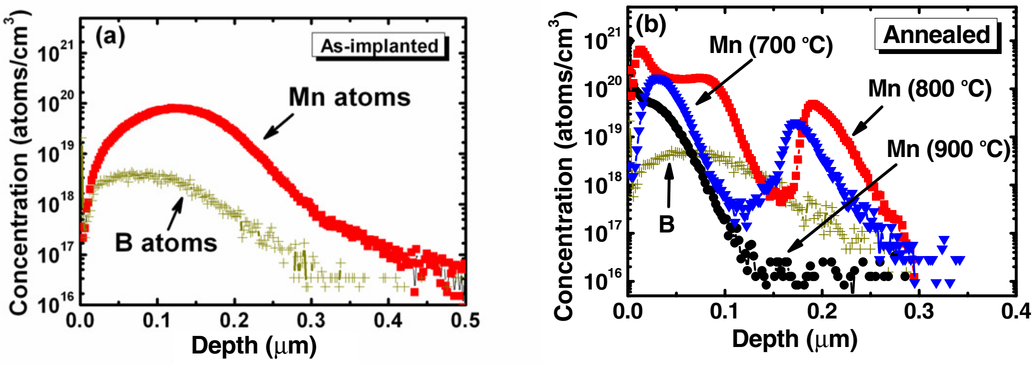

Figure 1. Depth profiles obtained by SIMS measurements of Mn and B concentrations in the $Si_{1-x}Mn_x$ samples ion implanted first with B at a dose of 5×10^{14} cm^{-2}, then with Mn at a dose of 1×10^{16} cm^{-2}: (a) Mn and B profiles in as-implanted $Si_{1-x}Mn_x$ samples; (b) B profile after annealing at 800 °C, and Mn profiles after annealing at 800 °C and 900 °C, respectively.

and importance of ion-implanted $Si_{1-x}Mn_x$ materials, in this study we carefully explore microstructures of ion-implanted $Si_{1-x}Mn_x$ samples via several complementary measurements, and hope to elucidate the origin of ferromagnetism in these materials.

2. Experimental methods

All samples (implanting targets) used in this study were prepared from well-cleaned p-type Si(100) wafers with an intrinsic B^+ ion concentration of 5×10^{15} cm^{-3}. Si substrates were first cleaned in acetone for 10 min, and dipped into diluted hydrofluoric acid (HF) for 1 min to remove the native oxide before the implantation processes. Sequential ion implantation was first performed at room temperature with additional B^+ ions at 25 keV with a dosage of 5×10^{14} cm^{-2}. Post-annealing was carried out at 900 °C for 150 s to avoid amorphization and to increase the concentration of itinerant carriers. The second implantation with Mn was performed at 150 keV with different dosages of 1×10^{15}, 5×10^{15}, and 1×10^{16} cm^{-2}. Finally, rapid thermal annealing was carried out at 700 °C, 800 °C, 900 °C, respectively, for 30 s to 1 min in a N_2 atmosphere in order to eliminate damage suffered from implantation and to activate implanted Mn^+ ions.

After the full process of ion implantation, we used secondary-ion mass spectroscopy (SIMS) to determine the distribution profiles of B and Mn in $Si_{1-x}Mn_x$ layers. Then, the magnetization properties were measured with a superconducting quantum interference device, or SQUID (MPMS-V, from Quantum Design Co. Ltd), at different temperatures. The magnetic field was applied parallel to the sample plane in this work because of the in-plane anisotropy of the samples. Furthermore, we combined the usage of a 200 keV transmission electron microscope, or TEM (JEOL 2010F), and energy dispersive x-ray spectroscopy (EDS) to pin down the microstructures and the determination of Mn concentrations at different locations. Finally, Hall measurements were performed at 15–300 K to examine the electrical properties of the Mn-implanted Si samples.

3. Results and discussion

In order to comprehend post-annealing effects, SIMS analysis was carried out to identify the concentration distribution of Mn element in the $Si_{1-x}Mn_x$ layers for as-implanted samples and those after annealing. Figure 1(a) shows the concentration profiles of Mn and B atoms in as-implanted $Si_{1-x}Mn_x$ samples with an Mn dose of 1×10^{16} cm^{-2}. The projected ranges of Mn and B atoms in as-implanted samples are around 130 and 110 nm, respectively, which are in good agreement with simulated results using the software code 'Transport of Ions in Matter' (TRIM) [30]. As shown in figure 1(b), annealing at 700 °C for 1 min or 800 °C or 900 °C for 30 s changes the concentration profiles of Mn atoms significantly. This is expected, since thermal diffusion of Mn atoms has been observed during annealing. On the other hand, the profiles of B atoms are relatively insensitive to the annealing process. Thus, we only show the profiles of B atoms annealed at 800 °C for 30 s for reference. It should be noted that Mn atoms tend to diffuse toward the free surface as the annealing temperature (T_A) increases. This leads to an overall lower Mn concentration for samples annealed at higher temperatures (see figure 1(b)).

The true excitement comes from the second peak in the Mn distribution at a depth of around 180–200 nm after annealing at 700 and 800 °C. This may indicate that a small amount of Mn atoms is trapped at the regime caused by radiation damage (vacancies, for instance), and that the tendency to diffuse toward the free surface is blocked. For samples annealed at 900 °C, the trapped Mn atoms gain enough thermal energy to diffuse out, and the concentration profile is monotonically decreasing without any observable second-peak feature.

Inspired by the dramatic difference in concentration profiles for T_A = 700, 800, and 900 °C, we measured the magnetization curves of $Si_{1-x}Mn_x$ by using the SQUID from 5 to 250 K at 1000 G, with an Mn dosage of 1×10^{16} cm^{-2} at different annealing temperatures. The diamagnetic signal from the Si substrate was subtracted and the magnetization was normalized by the surface area of the samples. As shown in figure 2, the separation between the zero-field-cooled (ZFC) and the field-cooled (FC) curves is manifest in

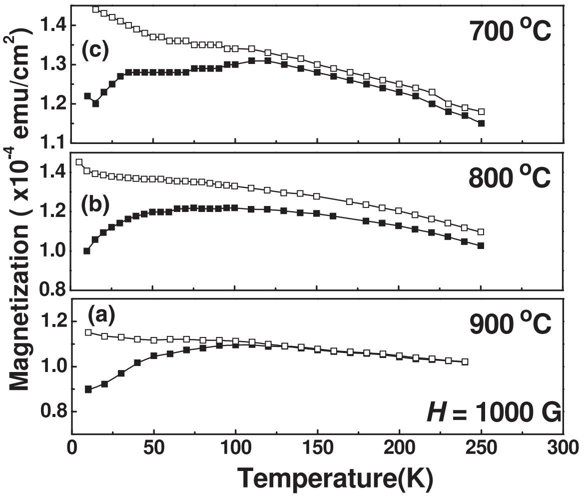

Figure 2. Magnetization versus temperature curves, ranging from 5 to 250 K, of the $Si_{1-x}Mn_x$ samples ion implanted first with B (5×10^{14} cm^{-2}) then with Mn (1×10^{16} cm^{-2}) and finally annealed at (a) 900 °C and (b) 800 °C and (c) 700 °C.

Table 1. Composition analysis by EDS at the places marked by numbers 1–6 in figures 4(a) and (b), respectively. Nos 1–4 indicate the round-shaped Mn-high precipitates; nos 5 and 6 indicate the matrix and Mn-lean clusters, respectively. The samples were ion implanted at a dose of 1×10^{16} cm^{-2} then annealed.

Annealing temperature (°C)	Composition	1	2	3	4	5	6
900	Si (at.%)	75.2	84.8	90.5	72.6	100	—
	Mn (at.%)	24.8	15.2	9.5	27.4	0	—
800	Si (at.%)	78.8	86.6	88.4	87.9	100	98.9
	Mn (at.%)	21.2	13.4	11.6	12.1	0	1.1

the low-temperature regime. The ZFC curves show a broad cusp in both samples, indicative of a characteristic blocking temperature (T_B) for superparamagnetic precipitates. These cup-like behaviors with temperature spanning from 50 to 125 K also indicate that the size distribution of superparamagnetic precipitates is rather broad. It should be noted that, for T_A = 900 °C, the ZFC and FC curves coincide with each other at around 130 K. However, at T_A = 700 and 800 °C, the ZFC and FC curves merge together only at temperatures well above 250 K. This hints at the presence of long-range ferromagnetic order above 250 K.

To confirm the ferromagnetic order, we resorted to the measurement of magnetization versus magnetic field (M–H) curves. Note that the hysteresis M–H curves shown in figure 3 exhibit different magnetic behaviors after different annealing conditions. For T_A = 900 °C, the hysteresis curve in figure 3(a) shows a ferromagnetic loop at 5 K but shrinks into a superparamagnetic response at higher temperatures. In the inset, we have enlarged the hysteresis loops near the zero-field regions, indicating the presence of superparamagnetic character at temperatures higher than T_B. On the other hand, for T_A = 800 °C, ferromagnetic characteristics are preserved up to at least 250 K, as is clearly shown in figure 3(b). The coercive fields measured at 5 K and 250 K are 380 G and 92 G, respectively. It is rather interesting that the existence of the second-peak structure in the SIMS profile seems to tight up to the observed ferromagnetism at high temperatures.

In order to elucidate the microstructure of the annealed samples and thus the origin of the ferromagnetism, we employed TEM/EDS analyses here. Figures 4(a) and (b) show the micrographs taken with TEM for Mn-implanted samples with a dosage of 1×10^{16} cm^{-2} and at T_A = 900 and 800 °C, respectively. Furthermore, composition analysis by EDS at different spatial points (marked by numbers in figure 4) is summarized in table 1. Four distinct features emerge. (i) nearly round-shaped precipitates with diameters ranging from 20 to 30 nm were found close to the surface for both T_A = 900 and 800 °C. These precipitates agglomerate and become larger with increasing T_A. The Mn concentrations in these round-shaped precipitates (nos 1–4) show a broad distribution between 10 and 27 at.%. (ii) In the matrix area (marked by no. 5), EDS shows 100% Si without any detectable Mn. (iii) For samples annealed at 800 °C, in addition to those round-shaped precipitates near the surface, there exists a thin layer with black contrast at a depth of about 180 nm

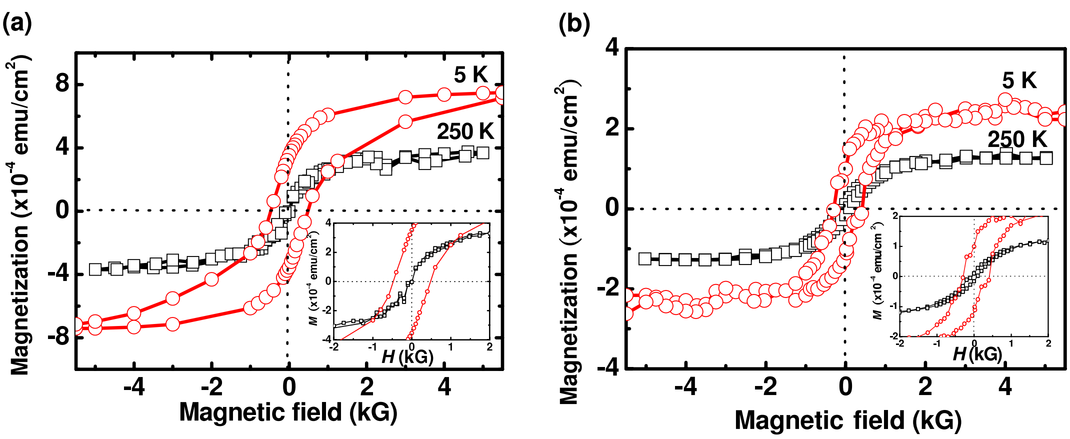

Figure 3. Magnetization versus magnetic field (M–H) curves, at 5 and 250 K, of $Si_{1-x}Mn_x$ samples ion implanted first with B (5×10^{14} cm^{-2}) then with Mn (1×10^{16} cm^{-2}) and finally annealed at (a) 900 °C and (b) 800 °C, respectively. Inset: the enlarged M–H loops near $H = 0$.

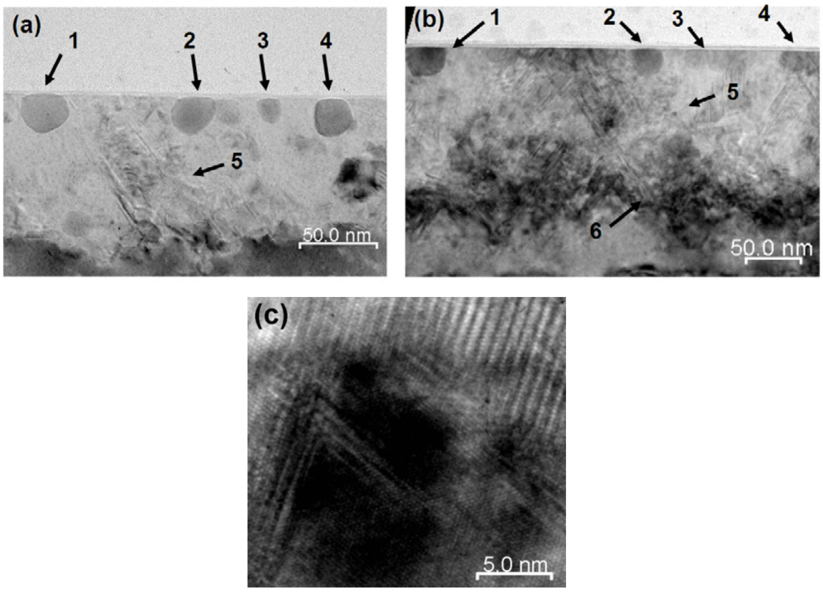

Figure 4. Cross-sectional TEM micrographs of $Si_{1-x}Mn_x$ samples ion implanted first with B (5×10^{14} cm^{-2}) then with Mn (1×10^{16} cm^{-2}) and finally annealed at (a) 900 °C and (b) 800 °C. (c) High-resolution TEM image of area marked by no. 6 in (b).

(no. 6), whose Mn content was analyzed to be 1.1 at.%. This layer is denoted as Mn-lean, which does not show up for $T_A = 900$ °C. (iv) Figure 4(c) demonstrates the high-resolution TEM (HRTEM) image of the region marked by no. 6 in figure 4(b). The image reveals high-quality crystal structure and low structure defects in this thin Mn-lean layer. No clear Mn-rich precipitates or Mn clusters were observed. Therefore, we believe that this thin Mn-lean layer could be regarded as a homogeneous layer.

It is rather worthwhile to point out that the depth position of the Mn-lean layer for $T_A = 800$ °C confirms the second peak of the concentration profile in previous SIMS results. The Mn content in this thin layer is too low to be manifested, and the black contrast in the TEM micrograph arises from implantation-induced defects which are not annihilated at $T_A = 800$ °C and below. Hence the formation of the Mn-lean layer is likely to be due to the remaining radiation damage, which becomes the sink to trap small amounts of implanted Mn atoms for low annealing temperatures. For $T_A = 900$ °C, the situation is rather different. The black contrast in corresponding depths does not show up any Mn content; Mn atoms gain enough thermal energy and diffuse to the surface, forming round-shaped precipitates, which is also consistent with the previous SIMS results. The second peak in the concentration profile after annealing has been observed in a similar experiment [20], in which high-temperature Mn implantation was adopted without additional B implantation.

In principle, both the localized carriers in impurity states and itinerant carriers in the host semiconductor bands will help to stabilize ferromagnetism. To differentiate their contributions, we resorted to transport measurements. First of all, electrical measurements at 300 K by the van der Pauw method showed that $Si_{1-x}Mn_x$ samples are p-type semiconductors. Figure 5 shows carrier concentrations with different Mn dosages at $T_A = 800$ and 900 °C. The Hall

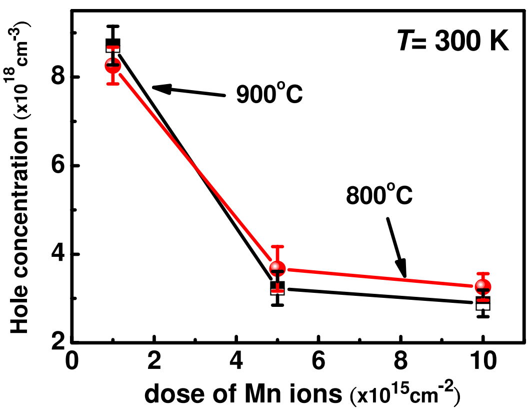

Figure 5. The dependence of hole concentration on implanted Mn doses and T_A.

measurements revealed that hole concentration decreases with increasing Mn dosage and only changes slightly with T_A. The dose-dependent trends show that the implanted Si samples with higher Mn dosages have more radiation-induced defects that trap itinerant carriers. In addition, high Mn doping in Si may also introduce several deep energy-level traps (>0.2 eV) to capture/recombine the itinerant carriers [31]. From figure 5, it is clear that the concentration of itinerant carriers is significantly suppressed by a factor of two when the implantation dosage goes up from 1×10^{15} to 1×10^{16} cm^{-2}. However, we do not see any corresponding weakening in the ferromagnetic properties.

In the case of the Mn-doped Si system (a prototypical IV-based DMS), Zhang *et al* [26] reported ferromagnetic films grown by a vacuum deposition method with a T_C higher than 400 K. More recently, Bolduc *et al* [19] and Kwon *et al* [22] also reported the intrinsic ferromagnetic behavior of Mn ion-implanted Si samples with T_C s higher than 400 and 70 K, respectively. Considering these inconsistent results between different research groups, detailed investigation of the structural properties is essential to clearly determine the presence of clusters or second phases. In this study, we attempted to clarify the origin of ferromagnetism in Mn-implanted Si DMSs. By precise exploration of the above microstructure analysis by TEM and corresponding EDS spectra, we see that the superparamagnetic responses in the magnetic study are due to the round-shaped precipitates, and the high-temperature ferromagnetism arises from the Mn-lean thin layer, which only exists for $T_A = 800\,^\circ\mathrm{C}$ or lower. This establishes the connection between the presence of the second-peak feature in the concentration profiles and the ferromagnetism observed in SQUID measurements. A rough estimate from the Mn concentration in the thin layer indicates that the average distance between each Mn atoms is about 1 nm, which is too far for significant direct exchange. This serves as a strong indication that the observed ferromagnetism is carrier-mediated. Furthermore, we also try to measure the anomalous Hall effect (AHE) in these samples at temperatures well below room temperature. But, even at $T = 20$ K, all samples show the ordinary linear behavior. This is probably due to the thin depth of the Mn-lean layer, so that only very few itinerant carriers couple to the ferromagnetic moments. Thus, we tend to conclude that the origin of the observed ferromagnetism mainly arises from indirect exchange mediated by *localized* carriers in the impurity states.

It is rather remarkable that the Mn-lean layer alone leads to a T_C higher than 250 K. To enhance further the T_C achieved here, one can try to increase the Mn content in the Mn-lean layer, which works for other DMSs such as (Ga, Mn)As [7], (Zn, Co)O [8–10], and Ge(Mn) [17, 18]. But, with the ion-implantation technique, we have more knobs to tune up T_C. By adjusting different sequential implantation energies or dosages of Mn^+ and B^+, we may modify the distribution profiles dramatically at different depths/places. A p–n DMS junction may form at specific locations if an n-type substrate and suitable masks are used. In addition, there is plenty of space to explore by varying the post-implantation annealing conditions. Since the notorious problem of the solubility limit for transition metal doping in semiconductors can be avoided by ion implantation, we believe that the preliminary success we achieved in our Mn_xSi_{1-x} samples can be further strengthened with bright potential in the future. Also, the thin ferromagnetic layer produced by the sequential implantation-annealing process can serve as a filter for perpendicular spin-injection.

It is worth point out that the analyzed Mn content, 1.1 at.% Mn, in our Mn-lean layer showing a high Curie temperature is nothing unique at all. Bolduc *et al* found the same 1.1% Mn in their ion-implanted Si films showing $T_C \sim 400$ K [19, 20]. Even in bulk Si(Mn) samples prepared by arc-melting Si with 0.5–1.5 at.% Mn, a T_C of 262 K was observed as the Mn content is 1.5 at.% [32]. Incidentally, in MBE-grown Mn-doped Ge films which were self-assembled onto a 'matrix top layer' of Ge (∼1 at.% Mn), $T_C > 400$ K was identified for those films with nano-columns of GeMn inside (with a high Mn content of ∼30 at.%) [17, 18]. The matrix layer should play an important role in being responsible for the transport of spin-carrying charges among the nano-columns rendering them room-temperature ferromagnetic.

Mn content of 1–1.5 at.% in Si or Ge may play a similar role to Mn content of 5–8 at.% in GaAs. However, this is bad news, depicting a less available magnetic moment than in the case of (Ga, Mn)As.

4. Conclusions

To sum up our work, $Si_{1-x}Mn_x$ samples were fabricated by sequential implantation of B then Mn ions into p-type Si(100) and subsequent annealing. Mn-rich precipitates (with 10–27 at.% Mn) always form near the surface after annealing and contribute to the superparamagnetic properties in the samples. But, only at an annealing temperature of 800 °C or lower, a thin Mn-lean layer (∼1.1 at.% Mn) shows up beneath the surface and leads to ferromagnetism well above 250 K. Microstructure analyses show that Mn atoms diffuse, gather, and form round-shaped Mn-rich precipitates near the surface for all samples annealed at 700–900 °C. However, a small amount of Mn was trapped at the radiation damage sites and formed the Mn-lean layer embedded in the matrix of $Si_{1-x}Mn_x$ when the annealing temperature was 800 or 700 °C. The magnetic characteristics of $Si_{1-x}Mn_x$ were found to be strongly affected by processing parameters such as the annealing temperature, the morphologies of the second phases, and so on. The origin of ferromagnetism arisen from the Mn-lean layer is likely to be due to indirect exchange mediated by localized carriers in the impurity states. The Mn content of 1–1.5 at%, having been reported separately several times by different groups to show room-temperature ferromagnetism, seems meaningful for Si-based DMS. Finally, the thin ferromagnetic layer produced by the sequential implantation-annealing process can serve as a filter for perpendicular spin-injection.

Acknowledgments

The authors are grateful to the National Science Council of the Republic of China for sponsoring this research under the grants NSC 94-2120-M007-012 and NSC 95-212-M007-008.

References

[1] Gregg J F, Petej I, Jouguelet E and Dennis C 2002 *J. Phys. D: Appl. Phys.* **35** R121
[2] Zutic I, Fabian J and Das Sarma S 2004 *Rev. Mod. Phys.* **76** (2)
[3] Ohno Y, Young D K, Beschoten B, Matsukura F, Ohno H and Awschalom D D 1999 *Nature* **402** 790
[4] Young D K, Johnston-Halperin E, Awschalom D D, Ohno Y and Ohno H 2002 *Appl. Phys. Lett.* **80** 1598
[5] Ohno H, Shen A, Matsukura F, Oiwa A, Endo A, Katsumoto S and Iye H 1996 *Appl. Phys. Lett.* **69** 363
[6] Tanaka M and Higo Y 2001 *Phys. Rev. Lett.* **87** 026602
[7] Ohno H 2000 *J. Magn. Magn. Mater.* **200** 110
Edmonds K W, Wang K Y, Campion R P, Neumann A C, Farley N R S, Gallagher B L and Foxon C T 2002 *Appl. Phys. Lett.* **81** 4991
Ku K C *et al* 2003 *Appl. Phys. Lett.* **82** 2302

[8] Sharma P, Gupta A, Rao K V, Owens F J, Sharma R, Ahuja R, Osorio Guillen J M, Johansson B and Gehring G A 2003 *Nat. Mater.* **2** 673
[9] Jung S W, An S J, Yi G C, Jung C U, Lee S and Cho S 2003 *Appl. Phys. Lett.* **80** 4561
[10] Lin H T, Chin T S, Shin J C, Lin S H, Hong T M, Hung R T, Chen F R and Kai J J 2004 *Appl. Phys. Lett.* **85** 621
[11] Chiba D, Sato Y, Kita T, Matsukura F and Ohno H 2004 *Phys. Rev. Lett.* **93** 216602
[12] Chiba D, Yamanouchi M, Matsukura F and Ohno H 2003 *Science* **301** 943
[13] Park Y D, Hanbicki A T, Erwin S C, Hellberg C S, Sullivan J M, Mattson J E, Ambrose T F, Wilson A, Spanos G and Jonker B T 2002 *Science* **295** 651
[14] Tsui F, He L, Ma L, Tkachuk A, Chu Y S, Nakajima K and Chikyow T 2003 *Phys. Rev. Lett.* **91** 177203
[15] Kazakova O, Kulkarni J S, Holmes J D and Demokritov S O 2005 *Phys. Rev.* B **72** 094415
[16] Cho S, Choi S, Hong S C, Kim Y, Ketterson J B, Kim B J, Kim Y C and Jung J H 2002 *Phys. Rev.* B **66** 033303
[17] Jamet M, Barski A, Devillers T, Poydenot V, Dujardin R, Bayle-Guillemaud P, Rothman J, Bellet-Amalric E, Marty A, Cibert J, Mattana R and Tatarenko S 2006 *Nat. Mater.* **5** 653
[18] Devillers T, Jamet M, Barski A, Poydenot V, Dujardin R, Bayle Guillemaud P, Rothman J, Bellet Amalric E, Cibert J, Mattana R and Tatarenko S 2007 *Phys. Status Solidi* a **204** 130
[19] Bolduc M, Awo-Affouda C, Stollenwerk A, Huang M B, Ramos F G, Agnello G and LaBella V P 2005 *Phys. Rev.* B **71** 033302
[20] Bolduc M, Awo-Affouda C, Stollenwerk A, Huang M B, Ramos F G, Agnello G and LaBella V P 2006 *Nucl. Instrum. Methods* B **242** 367
[21] Bolduc M, Awo-Affouda C, Ramos F G and LaBella V P 2006 *J. Vac. Sci. Technol.* A **24** 1648
[22] Kwon Y H, Kang T W, Cho H Y and Kim T W 2005 *Solid State Commun.* **136** 257
[23] Sobolev N A, Oliveira M A, Amaral V S, Neves A, Carmo M C, Wesch W, Picht O, Wendler E, Kaiser U and Heinrich J 2006 *Mater. Sci. Eng.* B **126** 148
[24] Bandaru P R, Park J, Lee J S, Tang Y J, Chen L H, Jin S, Song S A and O'Brian J R 2006 *Appl. Phys. Lett.* **89** 112502
[25] Wu H W, Tsai C J and Chen L J 2007 *Appl. Phys. Lett.* **90** 043121
[26] Zhang F M, Liu X C, Gao J, Wu X S, Du Y W, Zhu H, Xiao J Q, Zhu H and Xiao J Q 2004 *Appl. Phys. Lett.* **85** 786
[27] Zhang Y, Jiang Q, Smith D J and Drucker J 2005 *J. Appl. Phys.* **98** 033512
[28] Liu L, Chen N, Wang Y, Yin Z, Yang F, Chai C and Zhang X 2006 *J. Cryst. Growth* **291** 239
[29] Liu X C, Lu Z H, Lu Z L, Lv L Y, Wu X S, Zhang F M and Du Y W 2006 *J. Appl. Phys.* **100** 073903
[30] Ziegler J F, Biersack J P and Littmark U 1985 *The Stopping and Ranges of Ions in Solids* vol 1 (New York: Pergamon)
[31] Kikoin K A and Fleurov V N 1994 *Transition Metal Impurities in Semiconductors* (Singapore: World Scientific) pp 88–94
[32] Ma S B, Sun Y P, Zhao B C, Tong P, Zhu X B and Song W H 2006 *Solid State Commun.* **140** 192